

Color Plates

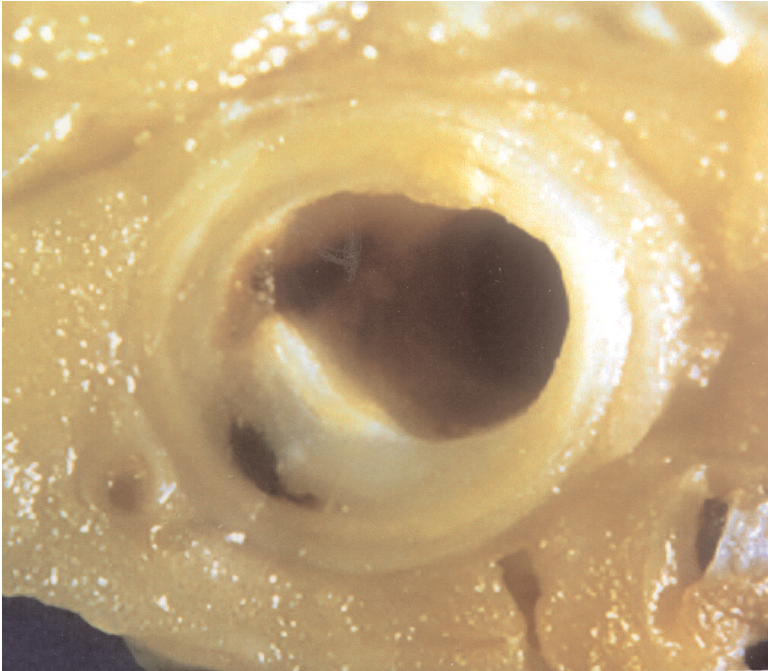


FIGURE 1.1. Atherosclerotic plaque in the artery.

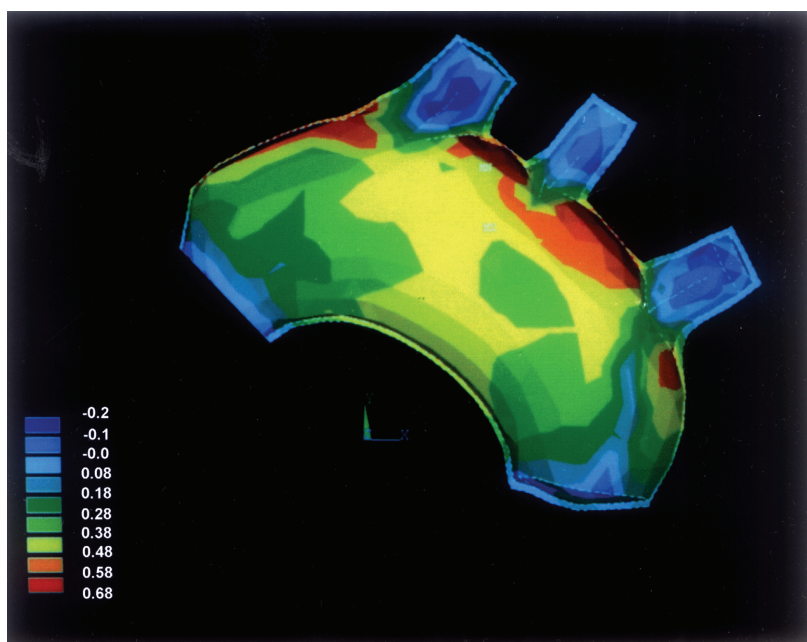
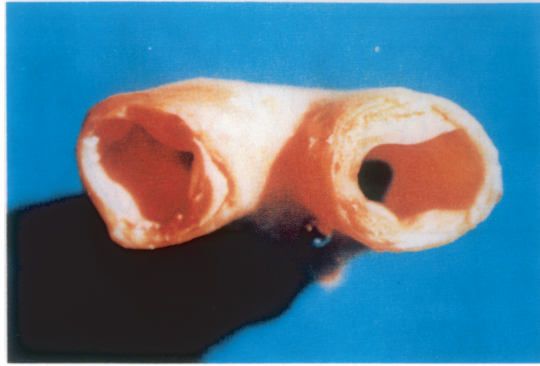
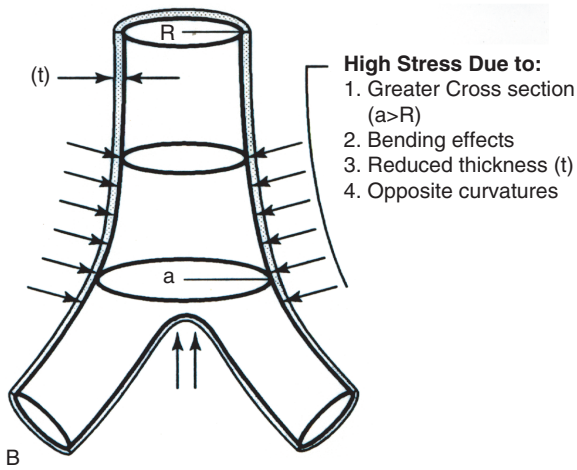


FIGURE 2.4. Circumferential strains in the human aortic arch and great vessels. The strains were determined for a pressure increase from 0 to 100 mmHg using a finite element analysis method. The strains are concentrated around the ostium of branches. See Chapter 7 for details.



A



B

FIGURE 2.5. (a) Photograph of a human aortic bifurcation showing atherosclerotic lesions at the crotch of the bifurcation. (Reproduced from Texon M, Hemodynamic Basis of Atherosclerosis. Hemisphere Publishing Corporation/Taylor & Francis Inc., Washington, DC, 1980, Plate 10A, with permission. All rights reserved.) (b) Schematic presentation showing various geometric parameters that may lead to uneven distribution of stress at the bifurcation. The stresses are high at both the crotch and the hip of the bifurcation.

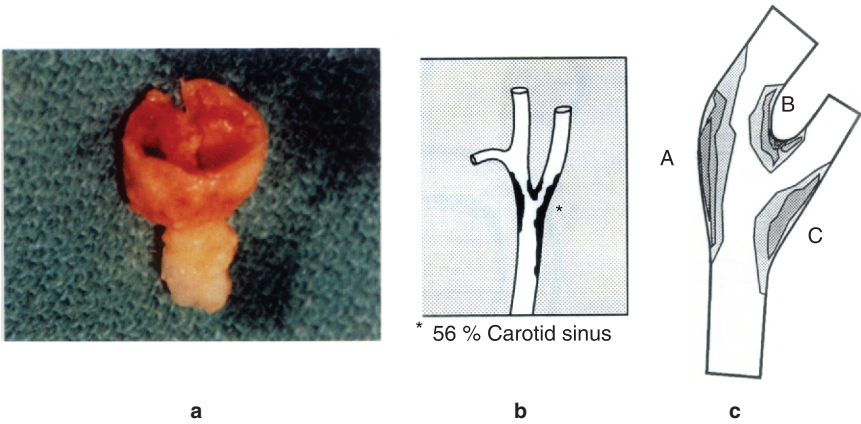


FIGURE 2.7. (a) Atherosclerotic plaque removed from a human carotid artery bifurcation. (b) Locations of atherosclerotic disease at the carotid bifurcation; 56% indicates the relative frequency of occlusive lesions in the brachiocephalic vascular system. Most often, the occlusive lesions occur involving the entire carotid bifurcation (a). (c) Maximum principal isostress contours at the human carotid artery bifurcation. The stresses are high at all three locations, B, A, and C, being the highest at B. The stress contours were obtained from the finite element analysis for a pressure (pulse) loading of 40 mmHg. See Chapter 6 for details.

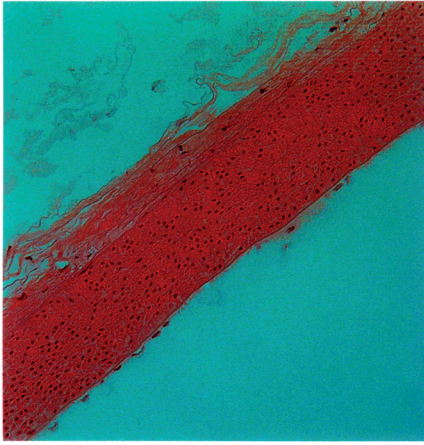
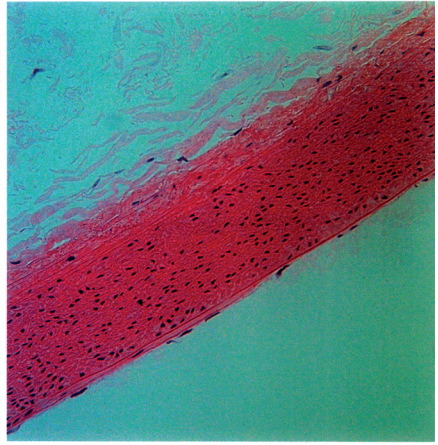
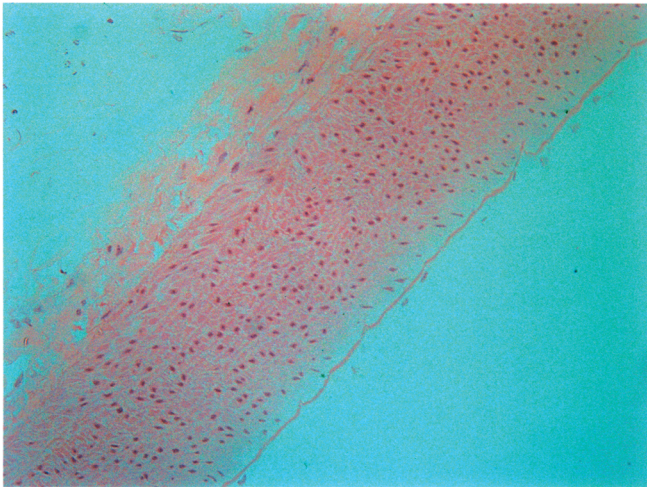
**Rabbit 32****Rabbit 29****Rabbit 30**

FIGURE 3.3. Longitudinal hematoxylin and eosin–stained sections of the rabbit abdominal aorta slightly away from the aortic bifurcation. The smooth muscle cells have been cut along their long axes as they are wound around the vessel.

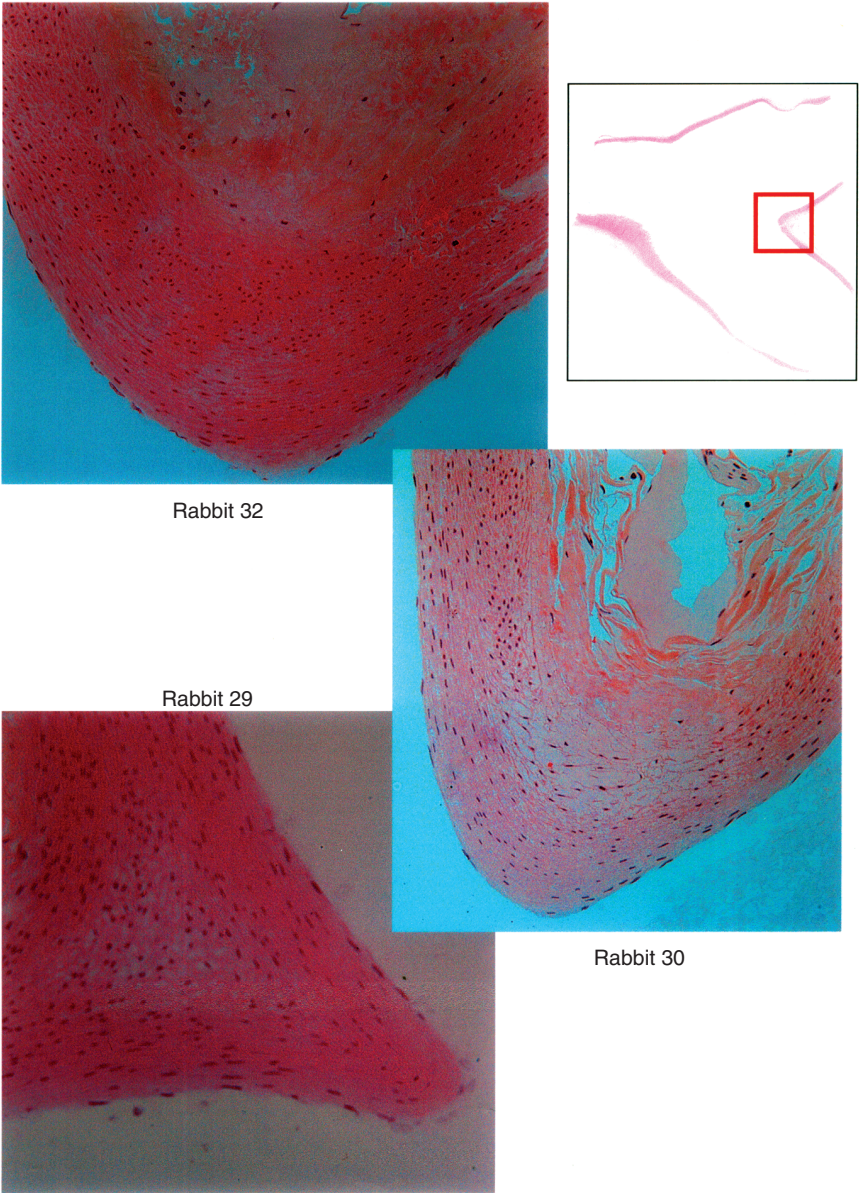


FIGURE 3.4. Longitudinal histological sections of the same aortas (shown in Fig. 3.3) but at the aortic bifurcation. The smooth muscle cells at the flow divider run in more than one direction and may even lie in more than one layer.

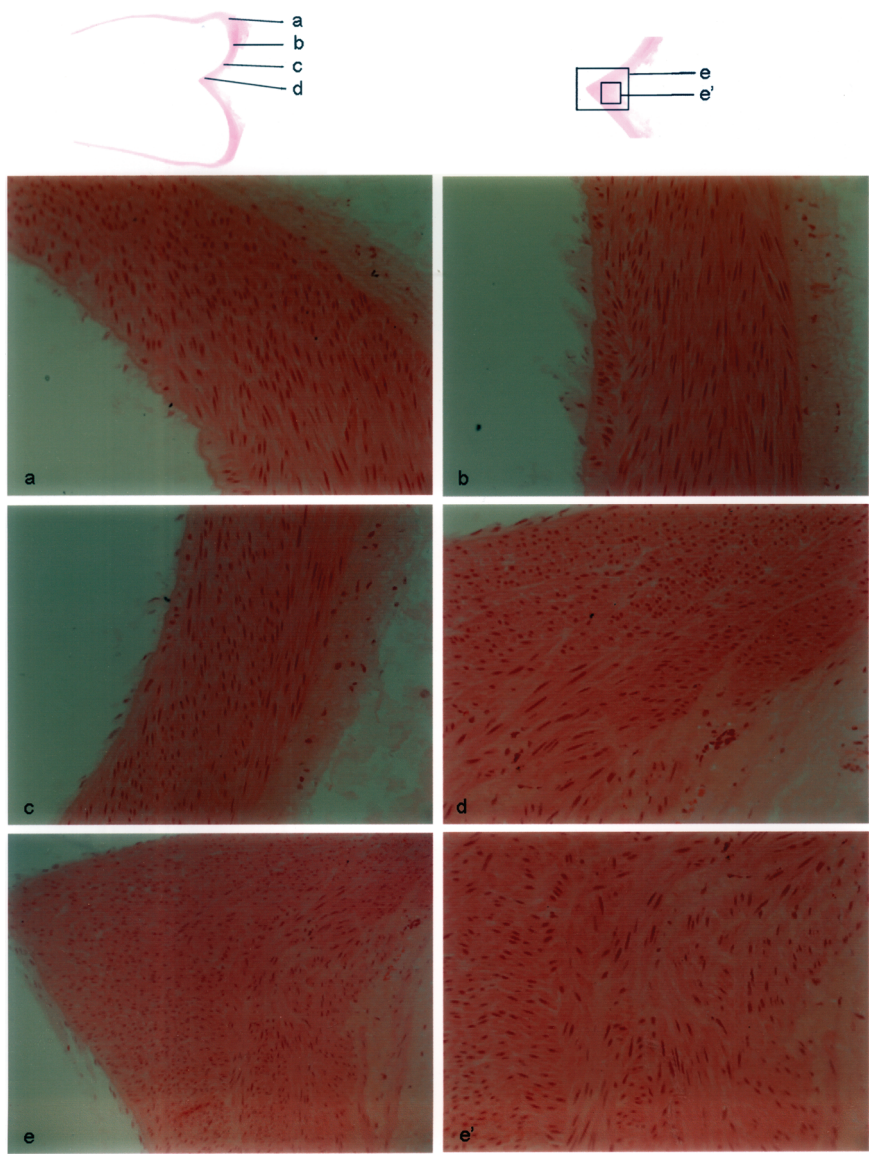
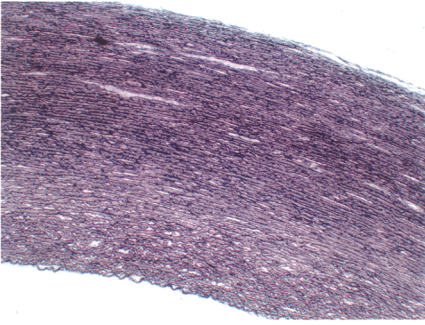
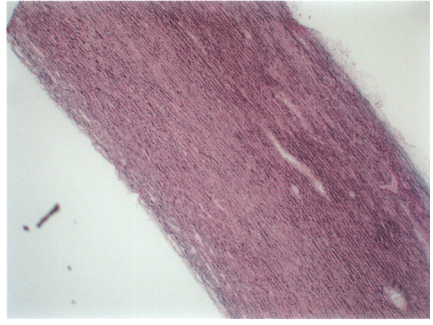


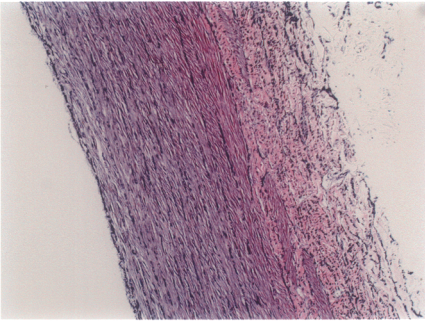
FIGURE 3.5. Longitudinal histological sections at and close to the aortic bifurcation in another rabbit. The smooth muscle cells appear to have more than one orientation, lie in multiple layers, and appear interwoven or braided.



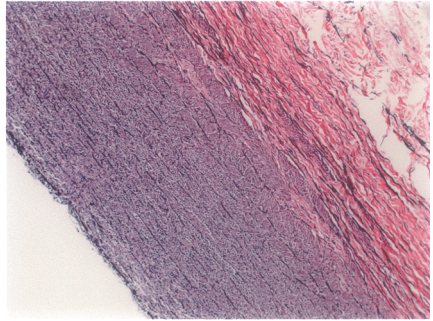
Pig Ascending Aorta, Transverse
Section (Approx. 40 x)



Pig Ascending Aorta, Longitudinal
Section (Approx. 40 x)



Pig Abdominal Aorta, Transverse
Section (Approx. 100 x)



Pig Abdominal Aorta, Longitudinal
Section (Approx. 100 x)

FIGURE 3.14. Verhoeff van Gieson–stained sections of porcine aortas. The elastin is stained black while smooth muscle cells are gray (usually yellow) and collagen fibers are red.

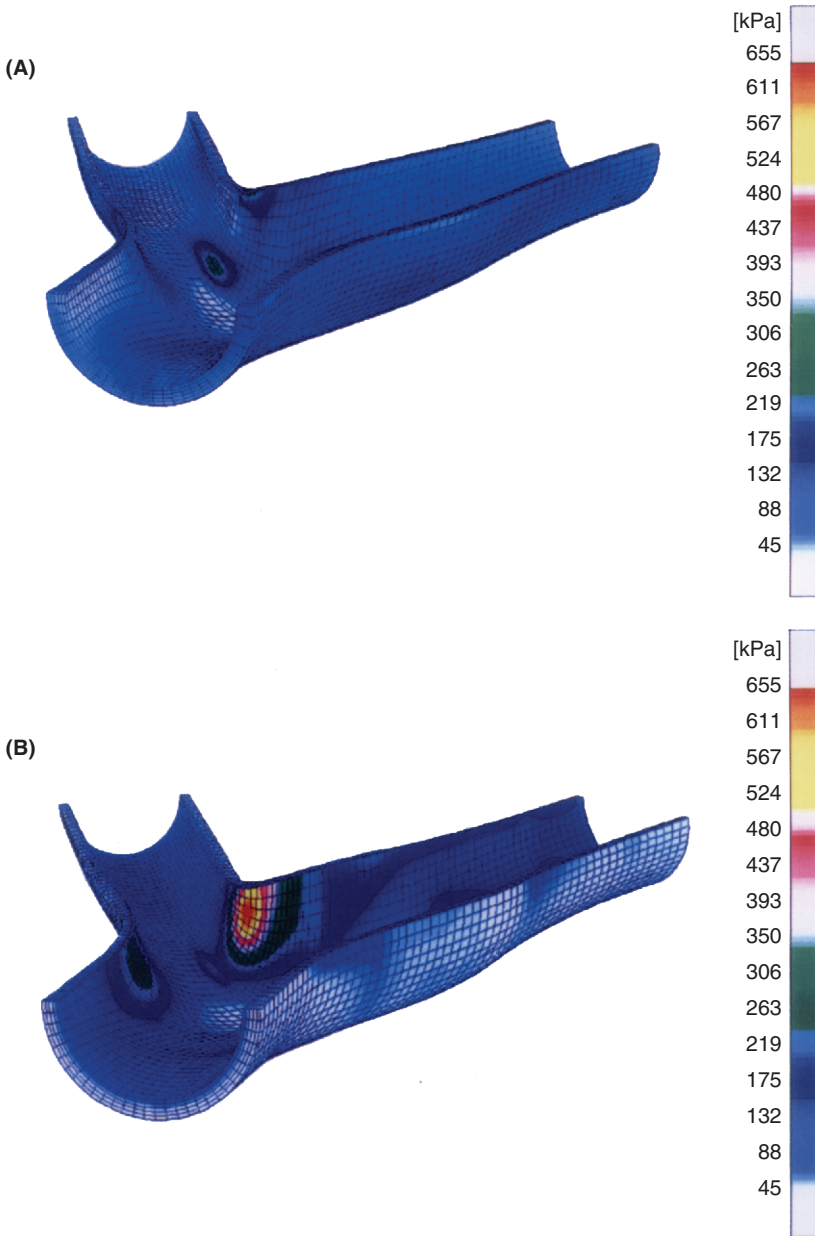


FIGURE 6.14. Maximum principal stress distribution at a pressure of 16 kPa (120 mmHg) with the residual strain (A) and without the residual strain (B) taken into account. The distribution of stress was made more uniform throughout the model geometry and through the wall thickness by the presence of residual strain (A). There is a concentration of stress at the apex, and the inner wall stresses are much higher without the residual strain (B). (Reproduced from Delfino A et al., J Biomechanics 1997;30:777-786, with permission.)

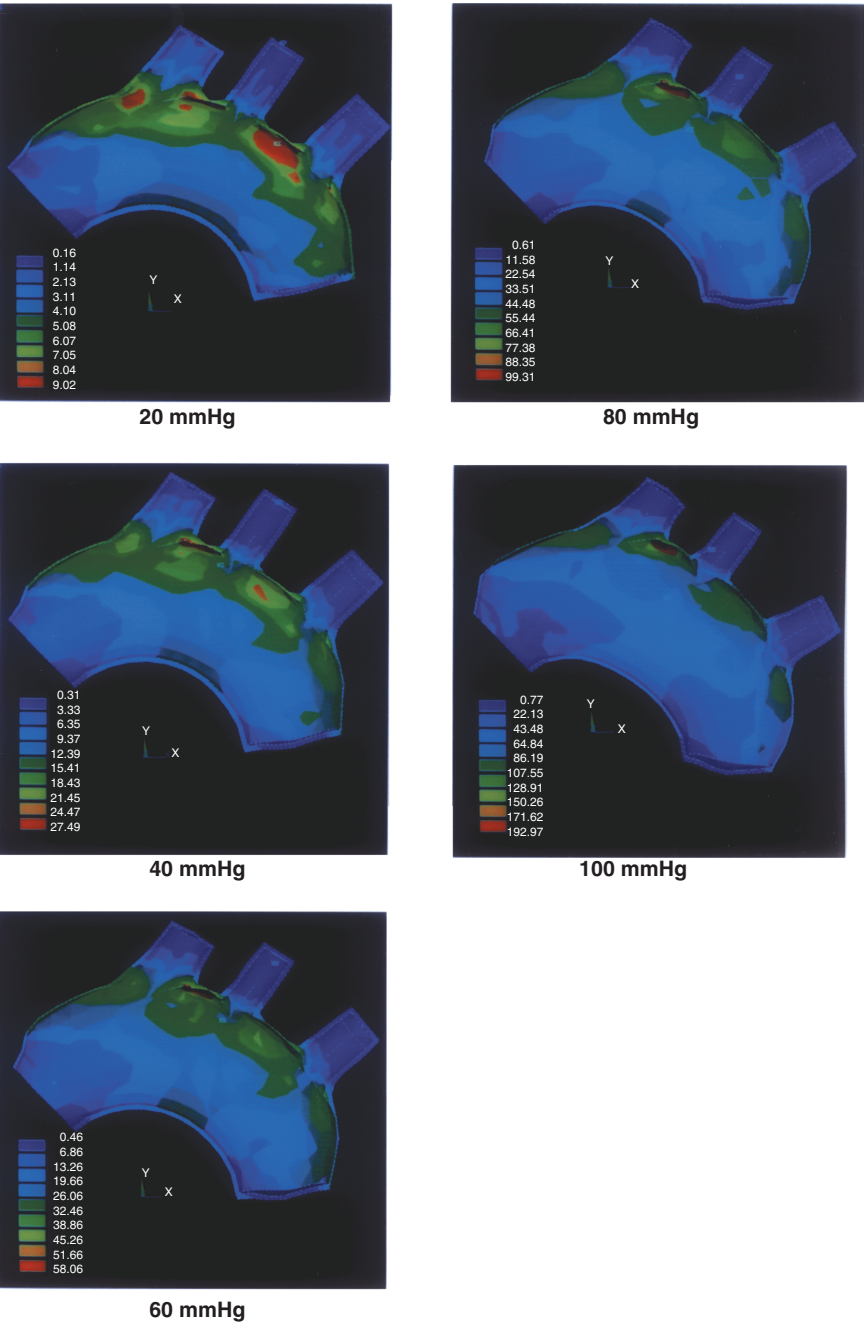
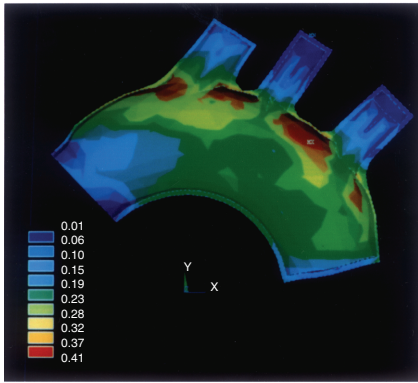
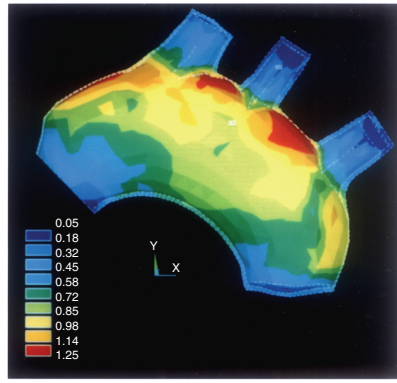


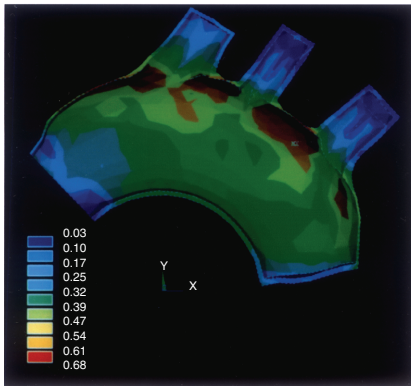
FIGURE 7.20. Equivalent stress (psi) on the inner surface of the aortic arch at various pressures. Stress-concentration is present around the branch ostium. Stress values are color-coded.



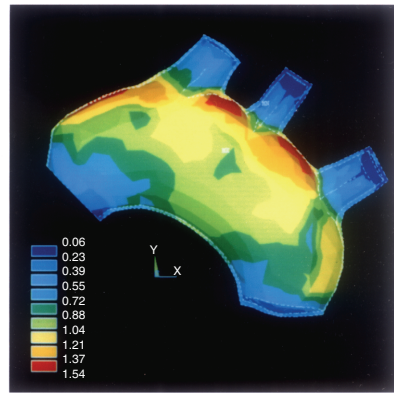
20 mmHg



80 mmHg



60 mmHg



100 mmHg

FIGURE 7.21. Equivalent strain (in./in.) on the inner surface of the aortic arch at various pressures. High strains can also be noted around the branch ostium. Strains are color-coded.

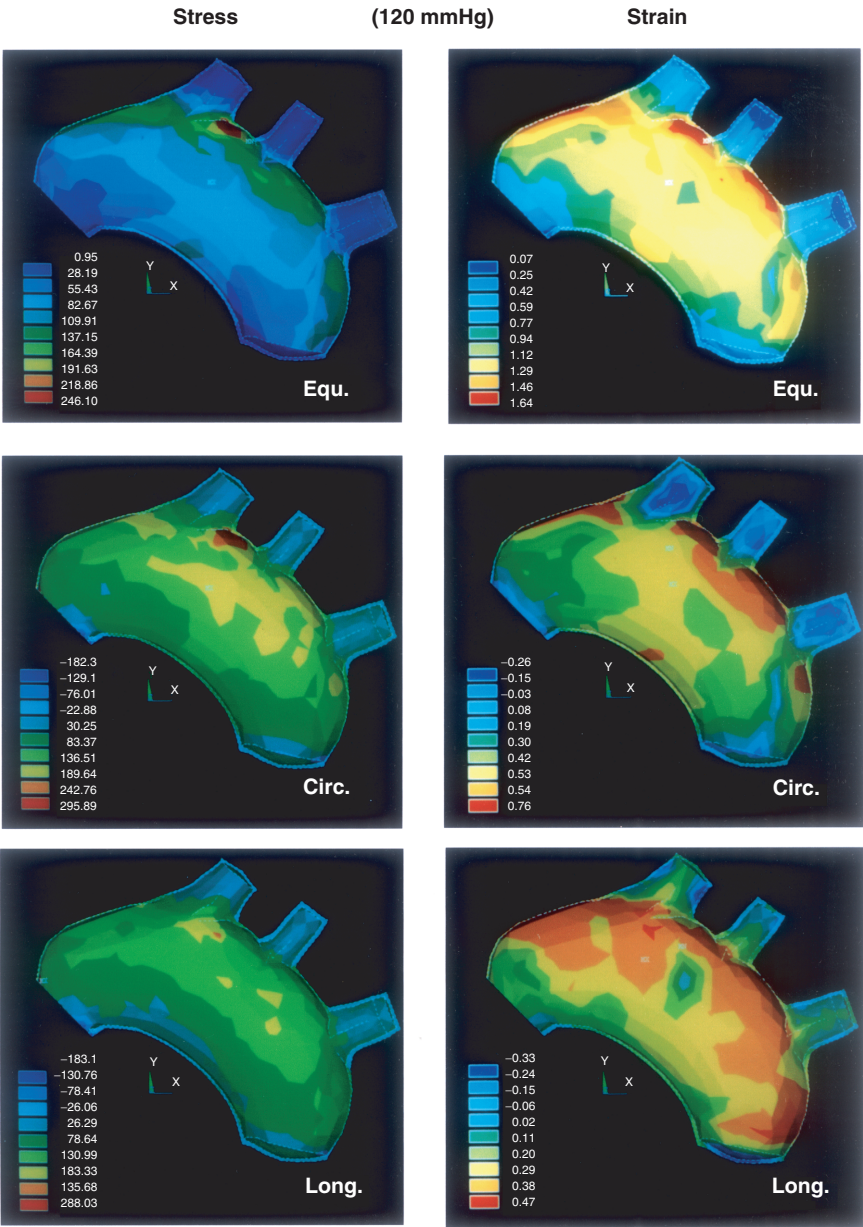


FIGURE 7.22. Stresses and strains on the inner surface of the aortic arch at 120 mmHg luminal pressure. Equ., equivalent; Circ., circumferential; and Long., longitudinal. Stresses are in psi and strains are in in./in.

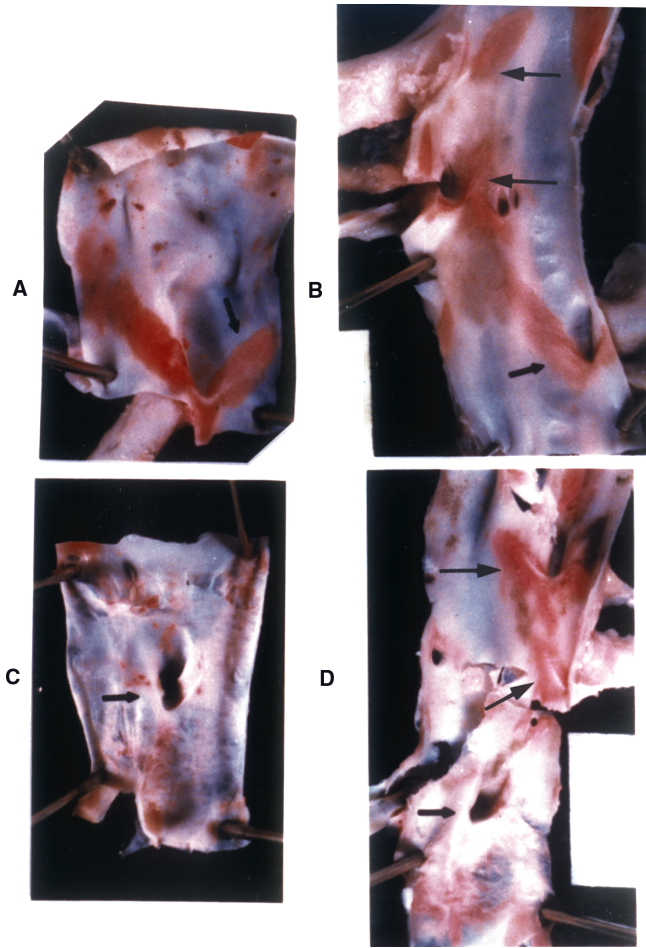


FIGURE 10.3. Photographs showing red atherosclerotic lesions at the arterial branches in three rabbits. Direction of blood flow is from top to bottom. In a rabbit on a high-cholesterol diet for 10 weeks, lesions developed on the superior mesenteric artery (a, arrow), whereas the casted left renal artery (c) was completely free of lesions (arrow). (b) In a rabbit on a high-cholesterol diet for 11 weeks, lesions developed on the left renal (bottom arrow), the right renal (middle arrow), and the superior mesenteric (top arrow) arteries. (d) In a rabbit on a high-cholesterol diet for 10 weeks, no lesions developed on the casted left renal artery (bottom arrow), whereas they did develop on the right renal (middle arrow) and superior mesenteric (top arrow) arteries.

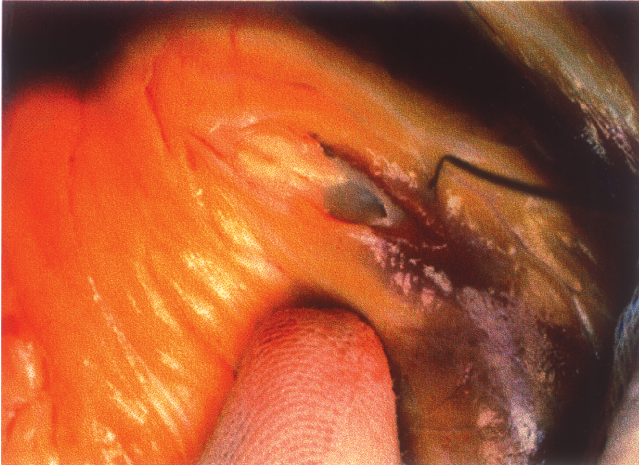


FIGURE 10.7. Photograph of the coronary artery in a patient taken intraoperatively. The coronary artery can be seen to go in the intramyocardial space. The incision in the myocardium exposes the place of entry of the coronary artery into the myocardium. The artery has developed severely occlusive atherosclerotic plaque in the epicardial segment but is completely normal and nonocclusive in the intramyocardial segment. The atherosclerotic lesion abruptly stops at the entry of the artery into the myocardium.

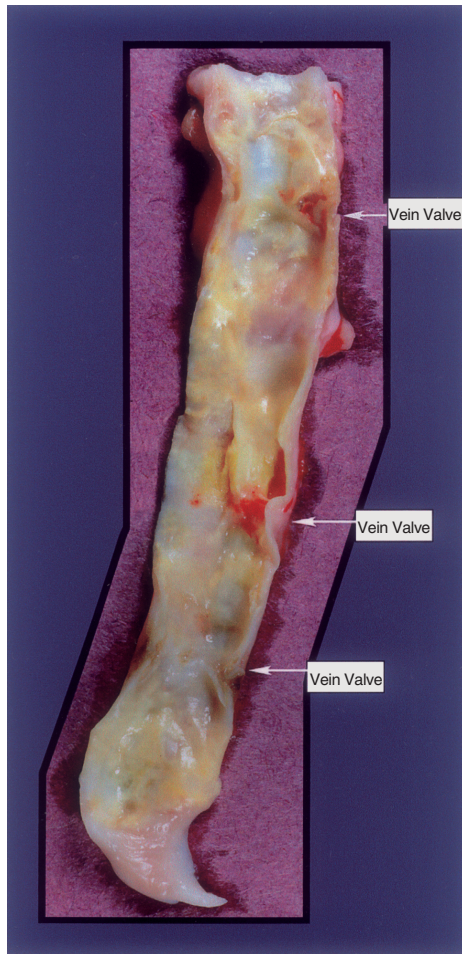


FIGURE 11.13. A vein graft removed (and opened) from a patient. All three locations where the graft developed blockages (arrows) are at the site of the vein valve.

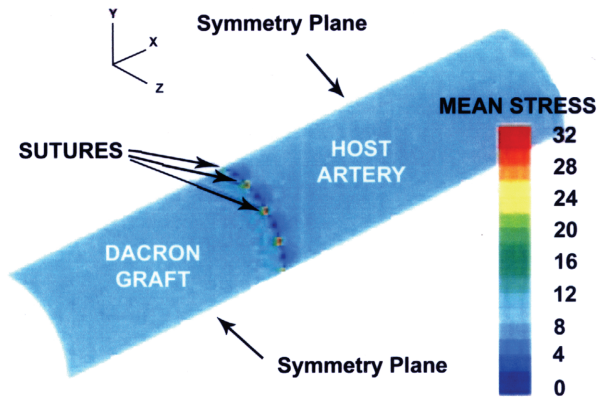


FIGURE 13.9. Mean stress distribution at the end-to-end Dacron graft–artery anastomosis projected onto a three-dimensional image of the geometry. Stress values are normalized by the inflating pressure and only one-quarter of the geometry is shown due to symmetry considerations. Stresses are concentrated equally at each suture attachment point, and the suture-induced stress concentrations are approximately eight times larger than stress values along the distal host artery. Similar results were obtained for the artery and vein grafts in this geometry. (Reproduced from Ballyk PD et al., J Biomechanics 1998;31:229-237, with permission.)

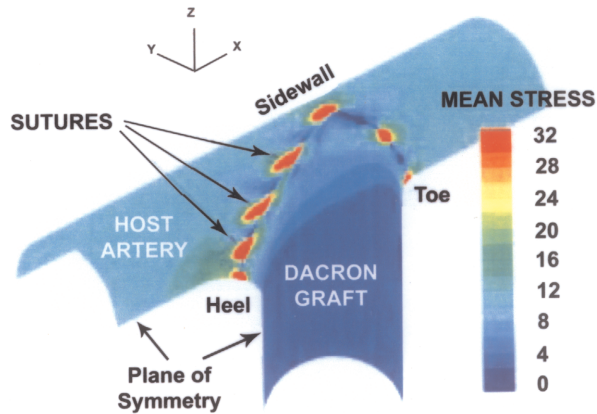


FIGURE 13.10. Mean stress distribution at the distal end-to-side Dacron graft–artery anastomosis projected onto a three-dimensional image of the geometry. Stress values are normalized by the inflating pressure and only one-half of the geometry is shown due to symmetry considerations. Stresses are concentrated at each suture attachment point, however, the stress-concentration at each suture is not the same. The suture-induced stress-concentrations range from 3 to 36 times the stress values along the distal host artery. Similar analyses were performed using artery and vein grafts in this geometry. (Reproduced from Ballyk PD et al., J Biomechanics 1998;31:229-237, with permission.)

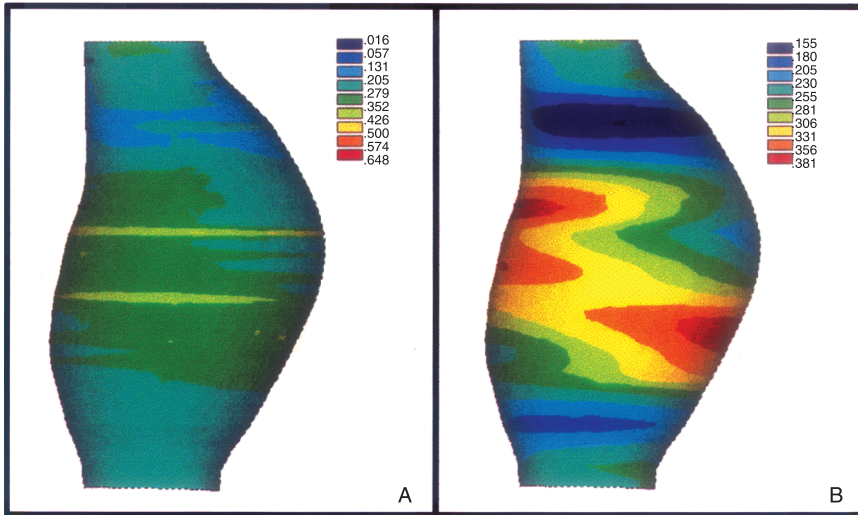


FIGURE 15.18. First principal stress (maximum stress) on inner surface (a) and middle surface (b) of aneurysmal aortic wall. Stress values are color-coded and shown in the inset in N/mm^2 . (a) On the inner surface, maximum stress occurs along two circumferentially oriented belts, one at the level of the bulb and the other just below the bulb. (b) Maximum stress occurs posteriorly at the bulb and anteriorly just below the bulb. Stress distribution is for luminal pressure of 120 mmHg.

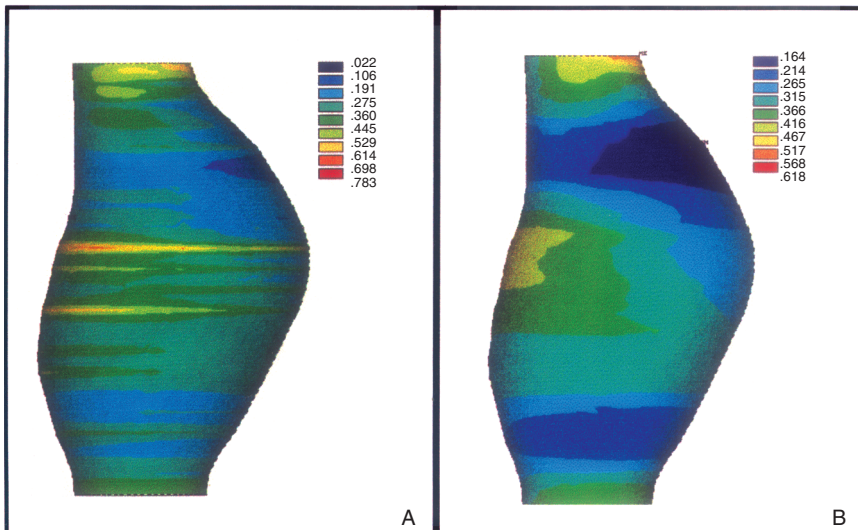


FIGURE 15.20. Maximum stress (first principal stress) on inner surface (a) and middle surface (b) of aorta for model in which luminal pressure and tethering force, which causes 5-mm increase in length, are applied. The stress distribution and orientation are altered substantially compared with that in the original model.

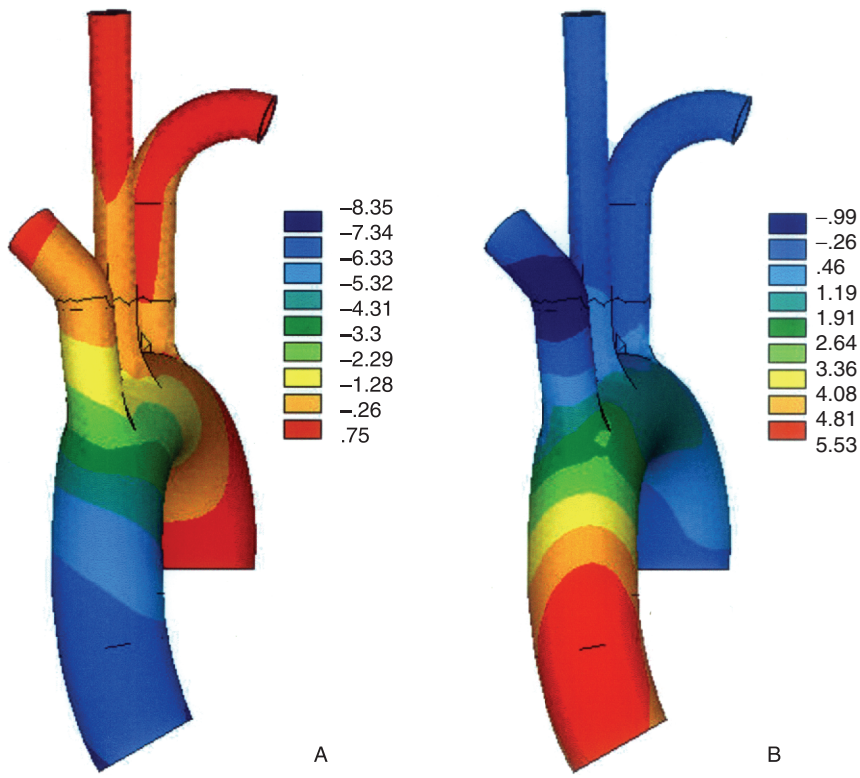


FIGURE 16.6. Displacement (mm) vertically downward (a) and perpendicular to the plane of the arch (b). In this model, the luminal pressure was 120 mmHg, the axial displacement was 8.9 mm, and the twist at the base was 6 degrees.

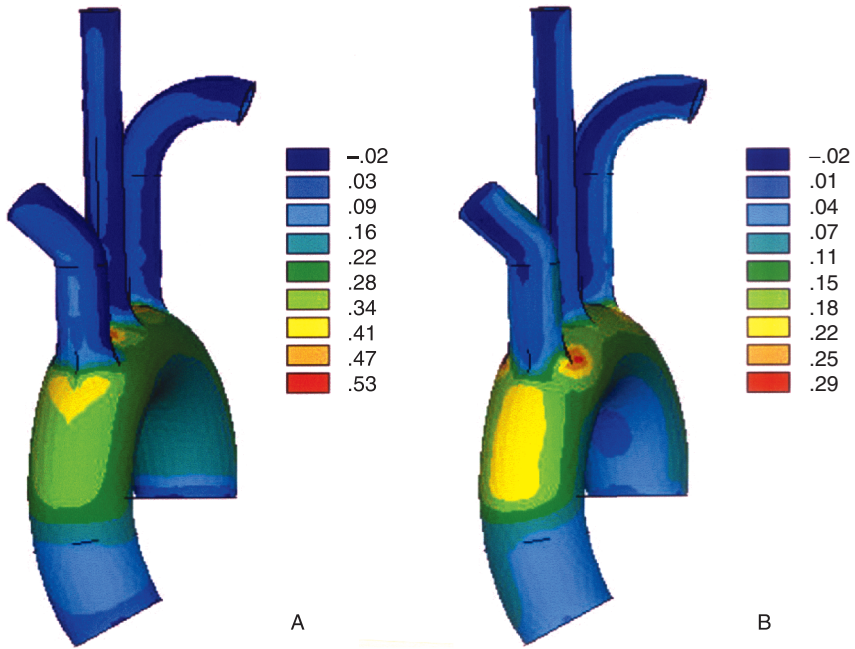


FIGURE 16.7. Distribution of circumferential (a) and longitudinal (b) stresses (N/mm²) in the aortic arch. In this control model, the only load was 120 mmHg luminal pressure. Expected stress-concentrations around the ostia of the supra-aortic vessels were observed.